

Anomalous Hall Effect and Magnetic Monopoles in Momentum-Space

Zhong Fang^{1,2*}, Naoto Nagaosa^{1,3,4}, Kei S. Takahashi⁵, Atsushi Asamitsu^{1,6}, Roland Mathieu¹, Takeshi Ogasawara³, Hiroyuki Yamada³, Masashi Kawasaki^{3,7}, Yoshinori Tokura^{1,3,4}, Kiyoyuki Terakura⁸

¹*Spin Superstructure Project (SSS), ERATO,
Japan Science and Technology Corporation (JST),
AIST Tsukuba Central 4, Tsukuba 305-8562, Japan;*

²*Institute of Physics, Chinese Academy of Science, Beijing 100080, China;*

³*Correlated Electron Research Center (CERC),
AIST Tsukuba Central 4, Tsukuba 305-8562, Japan;*

⁴*Department of Applied Physics, University of Tokyo,
7-3-1, Hongo, Bunkyo-ku, Tokyo 113-8656, Japan;*

⁵*DPMC, University of Geneva, 24,
quai Ernest-Ansermet, 1211 Geneva 4, Switzerland;*

⁶*Cryogenic Center, University of Tokyo,
2-11-16 Bunkyo-ku, Tokyo 113-0032, Japan;*

⁷*Institute for Materials Research, Tohoku University, Sendai 980-8577, Japan*

⁸*Research Institute for Computational Sciences (RICS),
AIST Tsukuba Central 2, Tsukuba 305-8568, Japan*

* To whom correspondence should be addressed. Email: z.fang@aist.go.jp

Efforts to find the magnetic monopole in real space have been made in cosmic rays and in accelerators, but up to now there is no firm evidence for its existence due to the very heavy mass $\sim 10^{16}\text{GeV}$. However, we show that the magnetic monopole can appear in the crystal-momentum space of solids in the accessible low energy region ($\sim 0.1 - 1\text{eV}$) in the context of the anomalous Hall effect. We report experimental results together with first-principles calculations on the ferromagnetic crystal SrRuO_3 that provide evidence for the magnetic monopole in the crystal-momentum space.

In 1931, Dirac [1] postulated the existence of magnetic monopole (MM) searching for the symmetry between the electric and magnetic field in the laws of electromagnetism. The singularity of the vector potential is needed for this Dirac magnetic monopole. Theoretically, the MM was found [2, 3] as the soliton solution to the equation of the non-Abelian gauge theory for the grand unification. However its energy is estimated to be extremely large $\sim 10^{16}\text{GeV}$, which makes its experimental observation difficult. In contrast to this MM in real space, one can consider its dual space, namely the crystal momentum (\mathbf{k} -) space of solids, and the Berry phase connection [4] of Bloch wavefunctions. This magnetic monopole in momentum space is closely related to the physical phenomenon, i.e., the anomalous Hall effect (AHE) in ferromagnetic metals.

The AHE is a phenomenon where the transverse resistivity ρ_{xy} in ferromagnets contains the contribution due to the magnetization M in addition to the usual Hall effect. The conventional expression for ρ_{xy} is

$$\rho_{xy} = R_0 B + 4\pi R_s M \quad (1)$$

where B is the magnetic field, R_0 is the usual Hall coefficient, and R_s is the anomalous Hall coefficient. This expression implicitly assumes that the additional contribution is proportional to the magnetization, and is used as an experimental tool to measure the magnetization as a function of temperature. Especially it is extensively used in the studies of ferromagnetic semiconductors with dilute magnetic impurities, which are the most promising materials for the spintronics [5]. However, the mechanism of AHE has been controversial for long [6, 7, 8, 9, 10]. The key issue is whether the effect is intrinsic or extrinsic and how to treat the impurity and/or phonon scatterings. Karplus and Luttinger [6] was the first to propose the intrinsic mechanism of AHE, where the matrix elements of the current operators

are essential. Other theories [7, 10] attribute the AHE to the impurity scattering modified by the spin-orbit interaction, namely the skew scattering [7] and/or the side-jump mechanism [10]. These extrinsic mechanisms are rather complicated and depends on the details of the impurities as well as the band structure. Nevertheless, all those conventional theories [6, 7, 8, 9, 10] for AHE derives Eq.1, as they are based on the perturbative expansion in the spin-orbit coupling (SOC) λ and the magnetization M , i.e., $R_s \propto \lambda$.

Recently the geometrical meaning of the AHE of the intrinsic origin [6] has been recognized by several authors [11, 12, 13, 14]. The transverse conductivity σ_{xy} can be written as the integral of the Berry phase curvature (gauge field) over the occupied electronic states in crystal momentum space (Eq.5 below). Magnetic monopole corresponds to the source or sink of the gauge field/curvature defined by this Berry phase connection. Therefore the AHE can be the direct fingerprint of the MM in crystal momentum space. Note here that the presence of the time-reversal symmetry results in $\sigma_{xy} = \rho_{xy} = 0$ in the d.c. limit from the very generic argument, and the group theoretical condition for the nonzero σ_{xy} is equivalent to that of finite ferromagnetic moment (see Supporting Online Material (SOM)). Therefore we need the ferromagnets to study σ_{xy} even though the Berry phase connection is more universal and exists even in nonmagnetic materials.

In this paper, we show by detailed first principles band calculation combined with the transport, optical, and magnetic measurements, that the observed unconventional behavior of the anomalous Hall effect and Kerr rotation in metallic ferromagnet SrRuO₃ is of intrinsic origin and is determined by the MM in \mathbf{k} -space. The conventional expression Eq.1 is invalidated by the experimental data presented below, showing the non-monotonous temperature dependence including even a sign change.

SrRuO₃ with the perovskite structure is an itinerant (metallic) ferromagnet. There are 4 t_{2g} electrons with the low spin configurations. The 4d orbitals of SrRuO₃ are relatively extended and the bandwidth is large compared with the Coulombic interaction. The relativistic SOC is also large in 4d electrons because of the heavy mass (of the order of 0.3eV for Ru atom). High-quality single crystal is available with the residual resistivity of the order of $10\mu\Omega\text{cm}$. These aspects make this system an ideal candidate to observe the AHE due to the \mathbf{k} -space gauge field. Stoichiometric SrRuO₃ (bulk and thin film) and Ca-doped (Sr_{0.8}Ca_{0.2}RuO₃ thin film) single crystals were prepared (see SOM for the details of sample preparation). The magnetization curve (Fig.1A) of SrRuO₃ film is quite similar to that of

bulk single crystal, except the Curie Temperature T_c ($\sim 150\text{K}$) is slightly lower than that of bulk ($\sim 160\text{K}$), due to the strain effects. On the other hand, the isovalent Ca-doping suppresses the T_c and magnetization M dramatically. All of the samples were used for the transport measurement in the d.c. limit. As seen from Fig.1C, the ρ_{xy} changes non-monotonously with temperature including even a sign change. Such behavior is far beyond the expectation based on the conventional expression Eq.1. In addition to the transport measurement, the frequency (ω) dependent conductivities (Fig. 2) were measured for SrRuO₃ film by optical method (see SOM). Except the strong structures around 3.0eV, which are mostly due to the charge transfer from O-2p to Ru-4d, sharp structures are also observed for both the real and the imaginary part of $\sigma_{xy}(\omega)$ below 0.5eV. Those low energy sharp structures cannot be fitted by extended Drude analysis. The lower the energy is, the stronger the deviations from fitting are. We will show, by combination with the first-principles calculations, that those unconventional behavior actually originate from the singular behavior of MM in the momentum space.

Now we turn to some details of the theoretical analysis. Berry phase is the quantal phase acquired by the wavefunction associated with the adiabatic change of the Hamiltonian [4, 15]. Let $|n(\alpha)\rangle$ be the n -th eigenstate of the Hamiltonian $H(\alpha)$ with $\alpha = (\alpha_1, \dots, \alpha_m)$ being the set of parameters, the Berry's connection is the overlap of the two wavefunctions infinitesimally separated in α -space, i.e.,

$$\langle n(\alpha)|n(\alpha + \Delta\alpha)\rangle = 1 + \Delta\alpha \cdot \langle n(\alpha)|\nabla_\alpha|n(\alpha)\rangle = \exp\left[-i\Delta\alpha \cdot \mathbf{a}_n(\alpha)\right]. \quad (2)$$

where the vector potential $\mathbf{a}_n(\alpha)$ is defined by $\mathbf{a}_n(\alpha) = i \langle n(\alpha)|\nabla_\alpha|n(\alpha)\rangle$. Although the concept of Berry phase has broad applications in physics [15], its relevance to the band structure in solids has been recognized only recently and in limited situations such as the quantum Hall effect under strong magnetic field [16] and the calculation of electronic polarization in ferroelectrics [17, 18]. In this case the parameter α is the crystal momentum \mathbf{k} . For the Bloch wavefunction $\psi_{n\vec{k}}(\vec{r}) = e^{i\vec{k}\cdot\vec{r}}u_{n\vec{k}}(\vec{r})$ with n denoting the band index and $u_{n\vec{k}}$ being the periodic part, the vector potential for the Berry phase $a_{n\mu}(\vec{k})$ is

$$a_{n\mu}(\vec{k}) = i \langle u_{n\vec{k}}|\frac{\partial}{\partial k_\mu}u_{n\vec{k}}\rangle. \quad (3)$$

With this vector potential, the gauge covariant position operator x_μ for the wavepacket made out of the band n is given by $x_\mu = i\partial_{k_\mu} - a_{n\mu}(\mathbf{k})$. Therefore the commutation relation

of x_μ 's includes the gauge field $F_{\mu\nu} = \partial_{k_\mu} a_{n\nu} - \partial_{k_\nu} a_{n\mu}$ as

$$[x_\mu, x_\nu] = -iF_{\mu\nu}. \quad (4)$$

which leads to the additional (anomalous) velocity $-i[x_\mu, V(x)] = -F_{\mu\nu}\partial V(x)/\partial x_\nu$ being transverse to the electric field $E_\nu = -\partial V(x)/\partial x_\nu$. Therefore the transverse conductivity σ_{xy} is given by sum of this anomalous velocity over the occupied states as [16]

$$\sigma_{xy} = \sum_{n,\mathbf{k}} n_F(\varepsilon_n(\mathbf{k})) b_z(\mathbf{k}). \quad (5)$$

where $b_z(\mathbf{k}) = F_{xy}(\mathbf{k})$ and $n_F(\varepsilon) = 1/(e^{\beta(\varepsilon-\mu)} + 1)$ (β : inverse temperature, μ : chemical potential) is the Fermi distribution function. Hence the behavior of gauge field $b_z(\mathbf{k})$ in k -space [19] determines that of σ_{xy} . One might imagine that it is a slowly varying function of \mathbf{k} , but it is not the case. Fig. 3B is the calculated result for $b_z(\mathbf{k})$ in the real system SrRuO₃. It has a very sharp peak near Γ -point and also ridges along the diagonals. The origin for this sharp structure is the (near) degeneracy and/or the band crossing, which act as MM. Consider the general case where two band Hamiltonian matrix $H(\mathbf{k})$ at \mathbf{k} can be written as $H(\mathbf{k}) = \sum_{\mu=0,1,2,3} f_\mu(\mathbf{k})\sigma_\mu$ where $\sigma_{1,2,3}$ are the Pauli matrices and σ_0 is the unit matrix. We can consider the mapping from \mathbf{k} to the vector $\mathbf{f}(\mathbf{k}) = (f_1(\mathbf{k}), f_2(\mathbf{k}), f_3(\mathbf{k}))$, and the contribution to σ_{xy} from the neighborhood of this degeneracy region is given by the solid angle $d\Omega_{\mathbf{f}}$ for the infinitesimal $dk_x dk_y$ integrated over \mathbf{k} . Therefore the gauge flux near the MM, namely the degeneracy point $\mathbf{f} = \mathbf{0}$ is singularly enhanced (as shown in Fig. 3). (See SOM for more details).

We studied the behavior of σ_{xy} by the first-principles calculations (see SOM for methods). The calculated density of states (DOS) is not so different between the cases with and without SOC (Fig.4A), while the σ_{xy} should be very sensitive to the Bloch wavefunctions and depends on the Fermi level position and the spin-splitting (magnetization) significantly, as predicted by above discussions. The behavior of σ_{xy} as a function of the Fermi-level position was obtained by using a small broadening parameter for the lifetime δ ($=70\text{meV}$) (Fig.4B). By shifting the Fermi level, not only the absolute value but also the sign of σ_{xy} is found to change. The sharp and spiky structures are just the natural results of singular behavior of MM (Fig.3). For the case without any shift of Fermi level, we obtain the value of $\sigma_{xy} = -60 \Omega^{-1}\text{cm}^{-1}$, which has the same sign as and is comparable with the experimental value ($\sim -100\Omega^{-1}\text{cm}^{-1}$). Such a spiky behavior should be also reflected in the ω dependent

σ_{xy} , especially for the low energy range with longer lifetime, while be suppressed at higher activation energy with shorter lifetime. As shown in Fig.2, for the ω dependence of optical conductivity, the high energy part ($>0.5\text{eV}$), which is dominated by the $p-d$ charge transition peak, is usual, and can be well reproduced by our calculations. While the observed peak structure of $\sigma_{xy}(\omega)$ below 0.5eV is the clear demonstration of the predicted spiky behavior. The spectra below 0.2eV is not measured due to the technical difficulty, but it is clear that even sharper structure should be there because the d.c. limit $\text{Re}(\sigma_{xy}) \approx -100\Omega^{-1}\text{cm}^{-1}$ has the opposite sign (the $\text{Im}(\sigma_{xy})$ at d.c. limit should go back to zero). Such a low energy behavior is well represented by our calculations, providing further evidence for the existence of magnetic monopoles.

Now it is straightforward to understand the results of transport measurement for σ_{xy} . Here we attribute the temperature (T) dependence of σ_{xy} to that of the magnetization $M(T)$. As the results of \vec{k} -space integration over occupied states, the calculated σ_{xy} is non-monotonous as a function of magnetization (Fig.1D). With the reduction of spin-splitting, the calculated σ_{xy} , after the initial increase, decreases sharply, then increases and changes sign becoming positive, and finally goes down again, capturing the basic features of the experimental results. Even more surprisingly, by converting the measured ρ_{xy} versus T curves shown in Fig.1C into the σ_{xy} versus M curves shown in Fig.1D, now they all follow the same trend, and match with our calculations as long as the experimental data is available. Those curves are measured for different samples (with different saturation moments), they all follow the same rule qualitatively, and could be simply explained by the reduction of magnetization [21] (see Fig.1A). Note, however, that the comparison between the experiments and calculations should be semi-quantitative, because the results are sensitive to the lattice structures. The calculated σ_{xy} for the fictitious Cubic structure shows a strong deviation from that obtained for orthorhombic structure, and it changes the sign to be positive at low temperature (large M). Therefore more accurate information on the structure is needed to obtain the quantitative result. However, such a sensitivity does not affect our main results, i.e, the non-monotonous behavior of σ_{xy} . Even the calculations for Cubic structure show such a behavior, and may be used as a guide of possible deviation.

The results and analysis presented here should stimulate and urge the reconsideration of the electronic states in magnetic materials from the very fundamental viewpoint. For example, the magnetic monopole is accompanied by the singularity of the vector potential,

i.e., Dirac string [1]. As shown by Wu-Yang [22] this means that more than two overlapping regions have to be introduced, in each of which the gauge of the wavefunction is defined smoothly. This means that one cannot define the phase of the Bloch wavefunctions in a single gauge choice when the magnetic monopole is present in the crystal momentum space. This leads to some nontrivial consequences such as the vortex in the superconducting order parameter as a function of \mathbf{k} [23], and many others are left for future studies.

-
- [1] P. A. M. Dirac, Proc. Roy. Soc. London **133**, 60 (1931).
- [2] G. t'Hooft, Nucl. Phys. B**79**, 276 (1974)
- [3] A. M. Polyakov, JETP Lett. **20**, 194 (1974).
- [4] It has been recognized in the original paper by M. V. Berry (Proc. R. Lond. **A392**, 45 (1984)) that the degeneracy point in the parameter space acts as a magnetic monopole where the gauge field is enhanced.
- [5] H. Ohno, SCIENCE, **281**, 951 (1998).
- [6] R. Karplus, J. M. Luttinger, Phys. Rev. **95**, 1154 (1954).
- [7] J. Smit, Physica **21**, 877 (1955); Physica **24**, 39 (1958).
- [8] W. Kohn, J. M. Luttigner, Phys. Rev. **108**, 590 (1957).
- [9] J. M. Luttigner, Phys. Rev.**112**, 739 (1958).
- [10] L. Berger, Phys. Rev. **B2**, 4559 (1970).
- [11] M. Onoda, N. Nagaosa, Phys. Rev. Lett. **90** 206601 (2003).
- [12] T. Jungwirth, Q. Niu, A. H. MacDonald, Phys. Rev. Lett. **88**, 207208 (2002).
- [13] Y. Taguchi, Y. Ohara, H. Yoshizawa, N. Nagaosa, Y. Tokura, Science **291**, 2573 (2001).
- [14] J. Sinova, T. Jungwirth, J.Kucera, A. H. MacDocnald, Phys. Rev. **B67**, 235203 (2003)
- [15] A. Shapere, F. Wilczek, *Geometric Phases in Physics*, (World Scientific, 1989).
- [16] D. J. Thouless, M. Kohmoto, M. P. Nightingale, M. den Nijs, Phys.Rev.Lett. **49**, 405 (1982).
- [17] R. M. Martin, Phys. Rev. B **5**, 1607 (1972).
- [18] R. D. King-Smith and D. Vanderbilt Phys. Rev. B. **47**, 1651 (1993).
- [19] Note that this gauge field is distinct from that of the magnetic field $\vec{B}(\vec{r})$ in real space, although they are analogous to each other. In the presence of $\vec{B}(\vec{r})$, the covariant momentum operator π_μ is given by $\pi_\mu = -i\partial_{x_\mu} + eA_\mu(\vec{r})$ where $\vec{B} = \nabla \times \vec{A}$. This leads to the commutation relation

$[\pi_x, \pi_y] = -ie(\partial_x A_y - \partial_y A_x) = -ieB_z$ etc., and to the Lorenz force due to the magnetic field \vec{B} . Therefore these two gauge fields, i.e., $b_\mu(\vec{k})$ and $\vec{B}(\vec{r})$, are dual to each other, and the presence of the one does not necessarily mean that of the other.

- [20] M. Shikano, T. K. Huang, Y. Inaguma, M. Itoh, T. Nakamura, Solid State Comm. **90**, 115 (1994).
- [21] More Ca-doped samples with different concentrations have been measured. They all follow the same trend, and are not shown here due to the space.
- [22] T. T. Wu, C. N. Yang, Phys. Rev. D **12**, 3845 (1975).
- [23] S. Murakami, N. Nagaosa, Phys. Rev. Lett. **90**, 057002 (2003).

Supporting Online Material

www.sciencemag.org

Supporting Online Text

References

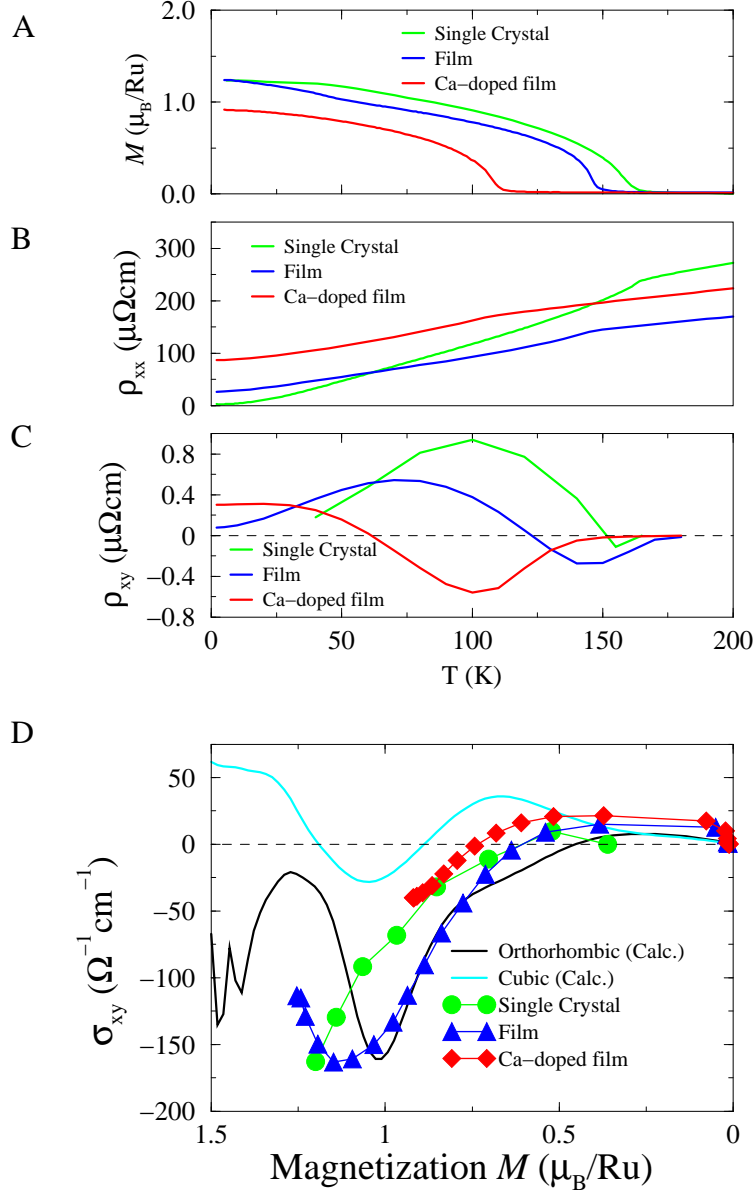


FIG. 1: Measured temperature dependence of the (A) magnetization M , (B) longitudinal resistivity ρ_{xx} , and (C) transverse resistivity ρ_{xy} for the single crystal and thin film of SrRuO₃, as well as for the Ca doped Sr_{0.8}Ca_{0.2}RuO₃ thin film. The corresponding transverse conductivity σ_{xy} is shown in (D) as a function of the magnetization, together with the results of first principle calculations for cubic and orthorhombic structures [20]. In our calculations, the change of magnetization is taken into account by the rigid splitting of up and down spin bands. As the transverse conductivity should vanish with M at high temperatures, the calculated σ_{xy} is multiplied by the additional M/M_0 ($M_0 = 1.5\mu_B$) factor, which does not affect its behavior except at the very vicinity of T_c .

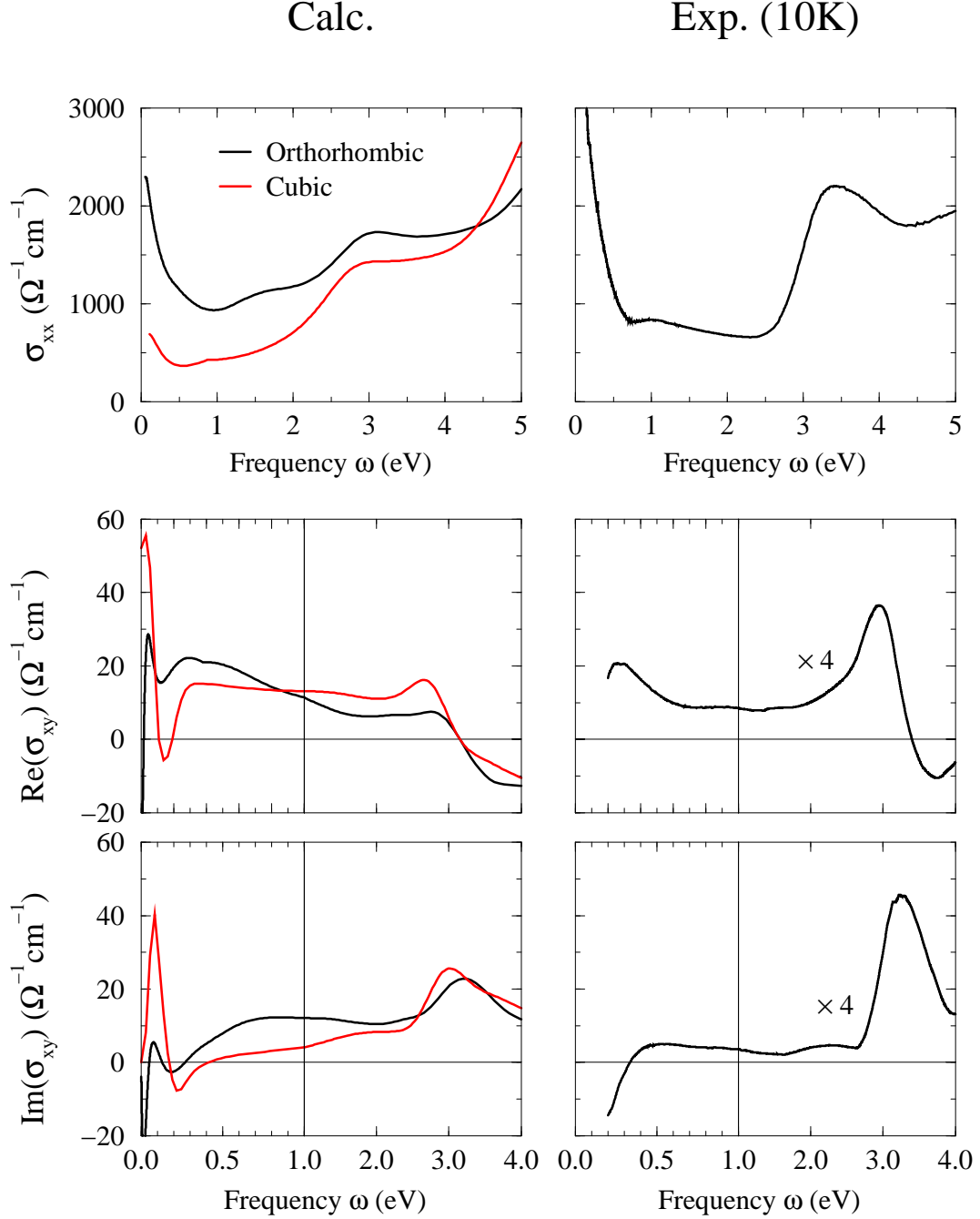


FIG. 2: Calculated (left panels) and measured (right panels) longitudinal (σ_{xx}) and transverse (σ_{xy}) optical conductivity of SrRuO₃ film. The measurements were performed at low temperature (10K). The calculations were done for both the orthorhombic single crystal structure and the hypothetic cubic structure by keeping the average Ru-O bond length. The experimental σ_{xy} are shown by multiplying a factor of 4. The quantitative comparison between the experiments and calculations about the absolute value of σ_{xy} would require more accurate structure information (see text part). Nevertheless, the clear peak structures for the low energy σ_{xy} is the demonstration of monopoles associated with $b_z(\mathbf{k})$.

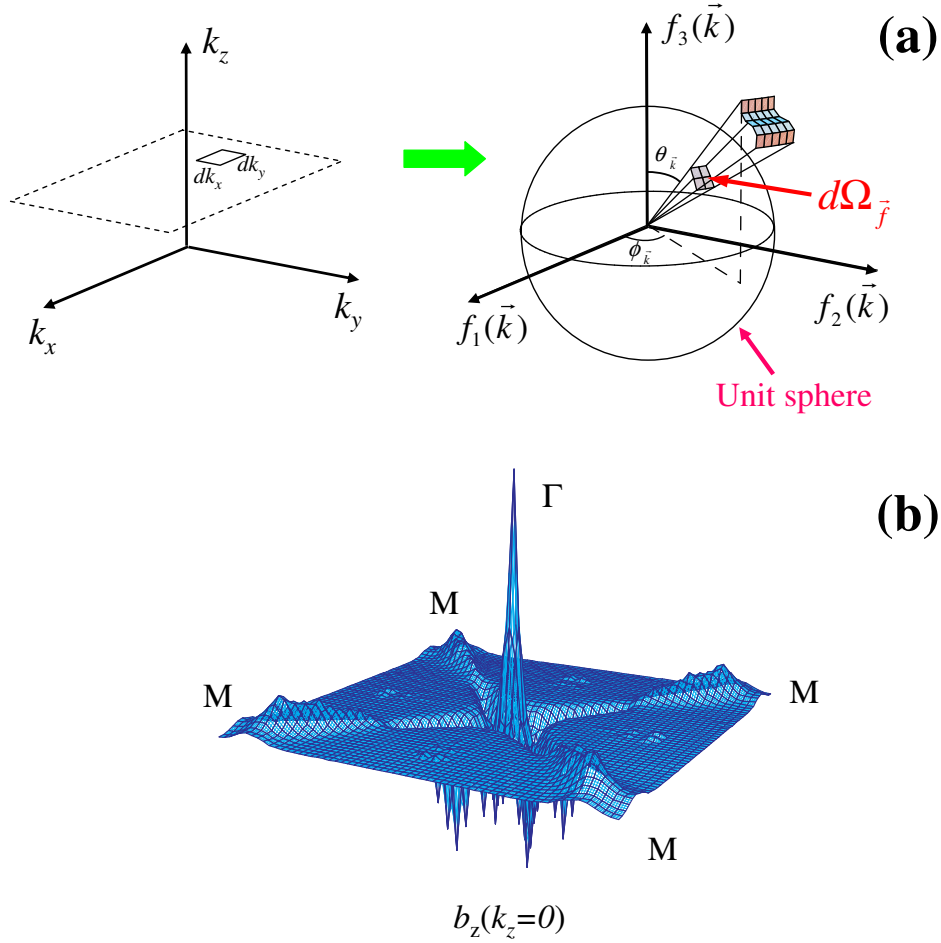


FIG. 3: (A) Geometrical meaning of the contribution σ_{xy} when the two bands are nearly degenerate. The two-dimensional Hamiltonian matrix $H(\vec{k})$ can be generally written as $H(\vec{k}) = \sum_{\mu=0,1,2,3} f_{\mu}(\vec{k})\sigma_{\mu}$ where $\sigma_{1,2,3}$ are the Pauli matrices and σ_0 is the unit matrix. By mapping from \vec{k} to the vector $\vec{f}(\vec{k}) = (f_1(\vec{k}), f_2(\vec{k}), f_3(\vec{k})) = f(\vec{k})(\cos \varphi_{\vec{f}} \sin \theta_{\vec{f}}, \sin \varphi_{\vec{f}} \sin \theta_{\vec{f}}, \cos \theta_{\vec{f}})$, the contribution to σ_{xy} from the neighborhood of degeneracy region can be given by the \vec{f} -space solid angle $d\Omega_{\vec{f}} = [\partial(\theta_{\vec{f}}, \varphi_{\vec{f}})/\partial(k_x, k_y)] \sin \theta_{\vec{f}} dk_x dk_y = d\varphi_{\vec{f}} \sin \theta_{\vec{f}} d\theta_{\vec{f}}$ for the infinitesimal $dk_x dk_y$ integrated over \mathbf{k} . The solid angle corresponds to the flux from the monopole at $\vec{f} = \vec{0}$. (See SOM). (B) Calculated flux distribution in \vec{k} -space for t_{2g} bands as a function of (k_x, k_y) with k_z being fixed at 0 for SrRuO₃ with Cubic structure. The sharp peak around $k_x = k_y = 0$ and the ridges along $k_x = \pm k_y$ are due to the near degeneracy of d_{yz} and d_{zx} bands because of the symmetry reasons as explained in the online supporting text.

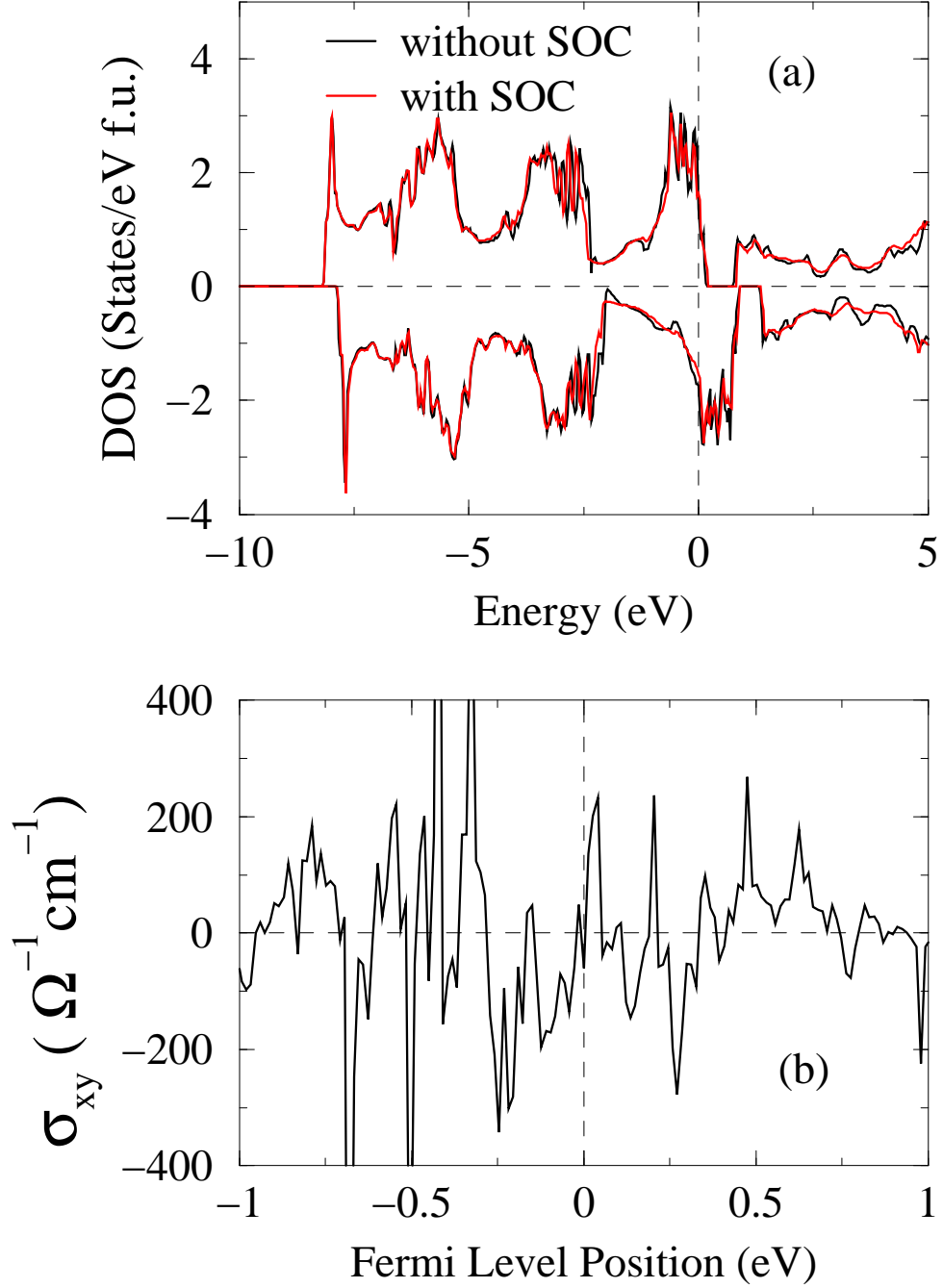


FIG. 4: The calculated (A) density of states (DOS) and (B) σ_{xy} as functions of Fermi level position for the orthorhombic structure of single crystal SrRuO_3 . The Fermi level is shifted rigidly relative to the converged solution, which is specified as zero point here. The sharp and spiky structure of σ_{xy} is the demonstration of the singular behavior of magnetic monopoles.

SUPPORTING ONLINE MATERIAL

Materials and Experimental Methods

Both stoichiometric SrRuO₃ and Ca-doped (Sr_{0.8}Ca_{0.2}RuO₃) thin (500Å) single crystal epitaxial films were grown on the (001) surface of SrTiO₃ (STO) single crystal substrate by pulsed laser deposition (PLD) employing KrF laser pulses (100mJ) focused on the polycrystalline target, while SrRuO₃ bulk single crystal were prepared using a flux method (SrCl₂ flux). The quality of those samples were confirmed by the X-ray diffraction. The bulk single crystal is orthorhombic, with $a=3.911\text{\AA}$, $b=3.936\text{\AA}$, $c=3.922\text{\AA}$. The films are coherently strained by the SrTiO₃ substrate, yielding a tetragonal distortion in the [001] direction. As the results, the out-of-plane lattice constants of films are elongated ($c=3.950\text{\AA}$ for SrRuO₃ film and $c=3.931\text{\AA}$ for Ca-doped film), and the magnetic easy axis is perpendicular to the film plane.

For the transport measurements of films, they were patterned in Hall bar geometry using conventional photo-lithography and Ar ion dry-etching. The Hall resistivity ρ_H was measured together with the longitudinal resistivity ρ_{xx} as a function of temperature under applied magnetic field. The anomalous resistivity ρ_{xy} was determined after subtraction of the ordinary Hall contribution from the measured ρ_H , and the transverse conductivity σ_{xy} was estimated as $-\rho_{xy}/\rho_{xx}^2$. In addition to the transport measurement, the frequency (ω) dependent conductivities were measured for SrRuO₃ film by optical method. The longitudinal part of the optical conductivity $\sigma_{xx}(\omega)$ was obtained from Kramers-Kronig transformation of normal reflectivity from 0.08eV to 40eV, while the transverse part $\sigma_{xy}(\omega)$ was deduced from magneto-optical Kerr spectra. The spectra were measured by a polarization modulation method. For the energy region of 0.7 – 4 eV, ordinary measurement system with grating monochromator and photo-elastic modulator (CaF₂ window, modulation frequency of 56 kHz) was used for the measurement. For the energy region below 0.8 eV, Fourier transform infrared (FT-IR) spectrometer with rapid scan mode (scan speed 0.16 cm/s) was utilized for the measurement. The light from the FT-IR interferometer was, at first, polarized by wire-grid polarizer (BaF₂ substrate). Then the polarization was modulated by ZnSe photo-elastic modulator (modulation frequency of 50 kHz) and focused by BaF₂ lens (focal length of 150 mm). The light reflected from the sample was detected by photovoltaic type

HgCdTe detector. By this system we can measure magneto-optical spectra down to 0.2 eV with accuracy higher than 0.01 degree.

Some Details of First-Principles Calculations

First-principles calculations of σ_{xy} are quite challenging, requiring the combination of several modern calculation techniques and powerful supercomputer sources. The plane-wave pseudopotential calculations [1] were performed based on the local spin density approximation (LSDA), that give good descriptions for the electronic and magnetic properties of this compound [2, 3]. The spin-orbital coupling (SOC) is treated self-consistently by using the relativistic fully separable pseudopotentials [4] in the framework of non-collinear magnetism formalism. The inter-band optical transitions are calculated from the converged Kohn-Sham eigen states by using the Kubo formula [5, 6]. The analytical tetrahedron method [7] has been used for the accurate \vec{k} -space integration, and the convergence has been checked carefully. The finite life-time broadening δ has been estimated from the experimental residual resistivity and extended Drude analysis of σ_{xx} . The validity of our calculation techniques has been well demonstrated in the explanation of anisotropic optical data in Ca_2RuO_4 [8].

σ_{xy} and Magnetic Monopole in Momentum Space

Here we present more details on the contribution to the transverse conductivity σ_{xy} from the \mathbf{k} region where two bands are nearly degenerate. Enhancement of the gauge field $b_z(\vec{k})$ occurs when more than two bands are close energetically, which corresponds to the magnetic monopole and shows its fingerprint in anomalous Hall effect (AHE) and Kerr rotation as described below [9]. Consider the general case where two band Hamiltonian matrix $H(\vec{k})$ at \vec{k} can be written as $H(\vec{k}) = \sum_{\mu=0,1,2,3} f_{\mu}(\vec{k})\sigma_{\mu}$ where $\sigma_{1,2,3}$ are the Pauli matrices and σ_0 is the unit matrix. Then we can consider the mapping from \vec{k} to the vector $\vec{f}(\vec{k}) = (f_1(\vec{k}), f_2(\vec{k}), f_3(\vec{k})) = f(\vec{k})(\cos\varphi_{\vec{f}}\sin\theta_{\vec{f}}, \sin\varphi_{\vec{f}}\sin\theta_{\vec{f}}, \cos\theta_{\vec{f}})$ as shown in Fig. 3A of the main text. Then $H(\vec{k})$ can be easily diagonalized to obtain the two eigenvalues $\varepsilon_{\pm}(\vec{k}) = f_0(\vec{k}) \pm f(\vec{k})$. Calculating Eq.5 of the main text in this case, we obtain the contribution to σ_{xy} from these two bands as

$$\sigma_{xy}^{2\text{-bands}} = \frac{e^2}{8\pi\hbar} \int d^3\vec{k} [n_F(\varepsilon_-(\vec{k})) - n_F(\varepsilon_+(\vec{k}))]$$

$$\begin{aligned}
& \times \left(\frac{\partial \varphi_{\vec{f}}}{\partial k_x} \frac{\partial \theta_{\vec{f}}}{\partial k_y} - \frac{\partial \varphi_{\vec{f}}}{\partial k_y} \frac{\partial \theta_{\vec{f}}}{\partial k_x} \right) \sin \theta_{\vec{f}} \\
& = \frac{e^2}{8\pi h} \int dk_z d\Omega_{\vec{f}} [n_F(\varepsilon_-(\vec{k})) - n_F(\varepsilon_+(\vec{k}))]. \tag{S1}
\end{aligned}$$

Here $d\Omega_{\vec{f}} = [\partial(\theta_{\vec{f}}, \varphi_{\vec{f}})/\partial(k_x, k_y)] \sin \theta_{\vec{f}} dk_x dk_y = d\varphi_{\vec{f}} \sin \theta_{\vec{f}} d\theta_{\vec{f}}$ is the \vec{f} -space solid angle, which is the integral of the gauge field

$$\vec{b}(\vec{f}) = \pm \frac{\vec{f}}{|\vec{f}|^3} \tag{S2}$$

due to the monopole at $\vec{f} = \vec{0}$ over the infinitesimal surface in \vec{f} -space corresponding to the small square $dk_x dk_y$ in \vec{k} -space (Fig.3A of the main text). Therefore $\sigma_{xy}^{2\text{-bands}}$ again has the geometrical meaning in \vec{f} space. This gauge field strongly depends on \vec{k} in the (near) degeneracy case, i.e., when $\vec{f}(\vec{k})$ is near the monopole.

There are two cases for the (near) degenerate bands. One is the accidental degeneracy [10, 11] where the three equations $f_1(\vec{k}) = f_2(\vec{k}) = f_3(\vec{k}) = 0$ are satisfied at $\vec{k} = \vec{k}_0$. Near this accidental band crossing, one can expand as $f_a(\vec{k}) = \sum_b \alpha_{ab}(k_b - k_{0b})$ where $a, b = 1, 2, 3$. In this case the \vec{f} -space can be identified with the \vec{k} -space, and the gauge field distribution in \vec{k} -space around $\vec{k} = \vec{k}_0$ is similar to Eq.S1 above replacing \vec{f} by $\vec{k} - \vec{k}_0$. Although there occurs no singularity in σ_{xy} at $\mu = \varepsilon_{\pm}(\vec{k}_0)$ due to the cancellation between the positive and negative $k_z - k_{z0}$, the nonlinear dependence of $f_a(\vec{k})$ gives rise to the strong μ -dependence of σ_{xy} slightly away from this energy. The other class of (near) degeneracy is due to the symmetry, where the \vec{k} -group has the irreducible representation with the dimensions more than 2. As an example, one can consider the simplest tight binding model of t_{2g} orbitals d_{yz} and d_{zx} on the cubic perovskite structure, which is relevant to the SrRuO₃ discussed in the main text. In this case the $H(\vec{k})$ for these two bands with up-spin is given by $f_0(\vec{k}) = -2t_1 \cos k_z - t_1(\cos k_x + \cos k_y)$, $f_1(\vec{k}) = 2t_2 \sin k_x \sin k_y$, $f_2(\vec{k}) = -\lambda M$, $f_3(\vec{k}) = -t_1(\cos k_x - \cos k_y)$, where t_1, t_2 are the effective intra- and inter-orbital transfer integrals respectively, λ is the spin-orbit coupling (SOC) constant, and M is the magnetization. When $\lambda M = 0$, there occurs the degeneracy along the line $\vec{k} = (0, 0, k_z)$. Furthermore when $t_2 = 0$, there occurs the degeneracy along the plane $k_x = \pm k_y$. Considering the case $t_1 \gg t_2 \gg \lambda M$, which is relevant to SrRuO₃, the gauge field $b_z(\vec{k})$ with $k_z = 0$ has a largest peak at $k_x = k_y = 0$ and is enhanced along the lines $k_x = \pm k_y$, which is actually seen in the realistic calculation for SrRuO₃ shown in Fig.3B of the main text. In this case there occurs no cancellation of $b_{nz}(\vec{k})$ from the integral over k_z .

Although the discussion above is applicable to any (near) degeneracy, the (singular) gauge field from different band crossings in \vec{f} -space cancel out in the presence of the time-reversal symmetry and/or the absence of the SOC. The former prohibits the finite σ_{xy} . In the absence of SOC, up-spin and down-spin bands are decoupled, and each of them can be represented by the Hamiltonian matrix without the time-reversal symmetry breaking. In ferromagnets with the SOC, the singular behavior of σ_{xy} by changing some parameters such as the chemical potential and the magnetization is the fingerprint of the monopoles in \vec{k} - and/or \vec{f} -space.



- [1] Z. Fang, K. Terakura, J. Phys.: Condens. Matt. **14**, 3001 (2002).
- [2] I. I. Mazin, D. J. Singh, Phys. Rev. B **56**, 2556 (1997).
- [3] D. J. Singh, J. Appl. Phys. **79**, 4818 (1996).
- [4] G. Theurich, N. A. Hill, Phys. Rev. B **64**, 73106 (2001).
- [5] C. S. Wang, J. Callaway, Phys. Rev. B **9**, 4897 (1974).
- [6] Z. Fang, N. Nagaosa, K. Terakura, Phys. Rev. B **67**, 35101 (2003).
- [7] P. Lambin, J. P. Vigneron, Phys. Rev. B **29**, 3430 (1984).
- [8] J. H. Jung, Z. Fang, J. P. He, Y. Kaneko, Y. Okimoto, Y. Tokura, Phys. Rev. Lett. **91**, 056403 (2003).
- [9] M. Onoda, N. Nagaosa, J. Phys. Soc. Jpn. **71(1)** 19(2002). In this paper, the magnetic monopole in momentum space has been discussed in relation to AHE for a simple two-dimensional model.
- [10] V. Neumann, E. Wigner, Physik. Zeits, **30**, 467 (1929).
- [11] C. Herring, Phys. Rev. **52**, 365 (1937).